PAPER

Check for updates

Unravelling the *in vivo* biotoxicity of a green-biofabricated graphene oxide–microplastic hybrid mediated by proximal intrinsic atomic interactions†

Adrija Sinha,[a] Sudakshya S. Lenka,‡[a] Abha Gupta,‡[a] Dibyangshee Singh,[a] Anmol Choudhury,[a] Shaikh Sheeran Naser,[a] Aishee Ghosh,[a] Faizan Zarreen Simnani,[a] Aditya Nandi, [ID][a] Richa Mishra,[b] Suresh K. Verma [ID] *[a] and Mrutyunjay Suar [ID] *[a]

Graphene oxide (GO) nanosheets have emerged as a potent nanomaterial for a range of applications, such as antibacterial and antibiofilm applications. Besides, microplastics are emerging as a chronic pollutant originating from the aggrandized usage of plastics, posing serious risks to living beings and the environment. In view of this issue, the individual toxicological impacts of GO nanosheets and polystyrene (PS) have received substantial research attention, yet the mechanistic details and toxicological effects of GO and PS combined in a hybrid system remain unknown. Hence, this study evaluated the *in vivo* biotoxicity of a lab mimic green-synthesized GO@PS hybrid using embryonic zebrafish through experimental and computational approaches. The physiochemical characterization of the GO@PS verified the synthesis of a stable 1433.0 ± 268.0 nm-sized GO@PS hybrid with a zeta potential of −47.3 ± 5.7 mV. Mechanistic analysis results deduced that the toxicological impact caused an induced apoptosis due to dysregulated oxidative stress led by the hypoxic condition created due to blockage of chorion by attachment and accumulation of GO@PS. The study elucidated the *in vivo* toxicity of GO, PS and GO@PS at cellular and molecular levels to devise measures for the safe usage of GO and PS in terms of environmental and human health aspects.

Environmental significance

The aggrandized use and advancement in research of graphene oxide-based materials and plastic materials have raised concerns about their after-usage wastes. These wastes lead to their accumulation in ecosystems, and potential toxicological impacts on environment. Hence, it is important to elucidate the comparative propensity of the biotoxicity of these compounds to prepare strategies for their eradication. This study describes their cellular and molecular biotoxicity using the embryonic zebrafish model. The graphene oxide–microplastic conjugates interact with different amino acids of cellular metabolic regulatory proteins like Sod1, tp53 and Zhe1a to display differential toxicity. This study has the potential to stimulate further investigations on biotoxicity and green approaches for the production of these materials and measures to safeguard environment.

1. Introduction

The research and development of nanotechnology has led to a new era of productivity and prosperity over the last decade.[1] Researchers have investigated a wide range of nanomaterials for different biomedical and environmental applications on grounds of their high reactivity owing to their higher surface area over other conventional materials.[2] An exponential evolution has been observed with regards to the preparation and synthesis of both organic and inorganic nanoparticles.[3] Among the different types of nanomaterials, graphene oxide has gained significant popularity owing to its large surface area and high adsorption capacity.[4] Its characteristic molecular and atomic features make it flexible for functionalization in different fields of application, like bioimaging,[5] biosensors,[6] gene and drug delivery,[7] and scaffold preparations.[8] At the molecular level, it can be defined as a carbon-based nanomaterial derivative of graphene, which comprises monolayer sp²-hybridized carbon atoms arranged in a hexagonal honeycomb lattice. This

[a] School of Biotechnology, KIIT University, Bhubaneswar, Odisha, 751024, India. E-mail: sureshverma22@gmail.com, msuar@kiitbiotech.ac.in

[b] Parul University, Waghodia, Vadodara, Gujarat, 391760 India

† Electronic supplementary information (ESI) available. See DOI: https://doi.org/10.1039/d4en00558a

‡ Authors with equal contribution.

arrangement imparts unique physiochemical properties that can serve various purposes.[9] Moreover, these features enhance the ability of graphene oxide to form hybrid materials with different types of other nanomaterials and compounds.[10,11] However, with the advancement in the research and development of graphene oxide and its derivatives at the lab scale and industrial level, its after-usage discharge in to the environment has also increased, which has led to concerns over its toxicological impact on human health and the environment.[12] Consequently, efforts have been made to study the toxicological impact of graphene oxide and its derivatives in different *in vitro* and *in vivo* models.[12] It has been reported that graphene oxide shows a mechanistic impact of different aspects of molecular toxicity at the cellular and organ levels.[12] Inferring from these information, it can easily be speculated that the after-usage graphene oxide that is accumulated in the environment could form hybrids with other xenobiotics and emerging contaminants, which could lead to hybrids that may exhibit toxicity in a synergistic or antagonistic manner at the biological level. Hence, an urgent detailed study for assessing the biomedical and ecological aspects is crucial.

With a size of less than 5 mm, microplastics (MPs) are evolving into a persistent emerging contaminant with serious repercussions for living beings and the ecosystem.[13] Numerous studies and research reports have shown the world-wide distribution of microplastics and their hazardous impacts on human health and the ecosystem in the last few years.[14–16] The toxicological impact of microplastics has been observed at every level of the food chain and ecosystems.[17,18] The severe effects of MPs have been caricatured due to their characteristic features of having a variety of shapes, colors, as well as variable chemical compositions, including comprising absorbents and additives.[19] Owing to their small size, MPs can be readily taken up by different organisms, leading to a concentration-dependent accumulation in their internal organs. The occurrence of MPs in the viscera, gills, and other tissues of aquatic animals, including mollusks, crustaceans, and fishes, has been widely reported.[20] MPs can generate a range of negative consequences in organisms, like decreased feeding activity, hindered growth and development, endocrine disruption, oxidative stress, genotoxicity, and even death.[21,22] In addition to this, the potentiality of MPs to penetrate food systems has led to rising concerns about human and environmental health and safety.[23] Serious toxicological consequences of MPs have also been observed in their synergistic combination with emerging contaminants, like nanomaterials.[24] It can be hypothesized that the accumulated MPs in the ecosystem at various levels, whether it be soil, water, or air, can form hybrid or composite materials with nanomaterials, like metal nanoparticles or organic nanomaterials like graphene oxide, in presence of natural conditions, like solar radiation, differential pH, and ionic disbalance.[25] Moreover, the presence of environmental factors (both biotic and biotic) acting as a catalyst for the combination of these nanomaterials can induce the process

of green synthesis naturally. Green-synthesized nanomaterials are generally preferred in scientific studies for their biocompatible properties;[26] however, there is a gap in information regarding the biological effects of naturally synthesized hybrid nanomaterials. These hybrid materials can further lead to actual impacts on human health and ecosystems in a synergistic or antagonistic manner and therefore require detailed investigations and reporting using both *in vitro* and *in vivo* models.

Zebrafish have gained enormous attention in the research field because of their multiple lab-friendly attributes, such as short life cycle, optical transparency at the embryonic and larval levels, and high genetic and anatomic similarity to humans with similar cellular metabolic activities.[27,28] There are numerous literature reports on toxicological as well as biomedical studies on different nanomaterials and emerging contaminates, like MPs, using embryonic and adult zebrafish as an *in vivo* model.[29,30] Studies have revealed the toxicity of graphene oxide on zebrafish embryogenesis at the molecular level, depicting the serious effect of graphene oxide exposure on development, physiology, and cellular death in zebrafish embryos.[31,32] Similarly, reports based on the cytotoxic effects of MPs and bisphenol conjugates indicated they had a concentration-dependent mortality effect on zebrafish larvae. Moreover, histological tests and transcriptome profiling on MP-exposed fish indicated the MPs had a significant effect on inflammatory response in the target tissues.[33] With reference to these results, it could be hypothesized that graphene oxide in combination with MPs could exhibit a synergistic and comparative toxicological impact at the cellular and molecular levels, which thus needs to be investigated by a scientific approach.

In view of unraveling the information about the combined and comparative toxicity of graphene oxide (GO) and microplastics (MPs), especially polystyrene microplastic (PS), a computational and experimental study was designed to mimic the formation of GO and PS hybrid material at the lab scale. Their combined toxicity was evaluated in comparison with the toxicity impacts of GO and PS at the cellular and molecular levels. The information obtained was speculated could answer the raised concerns about the synergistic toxicity of GO and PS, using embryonic zebrafish as an *in vivo* model, and could provide new insights for future toxicological research.

2. Experimental section

2.1. Synthesis of graphene oxide–polystyrene microplastic (GO@PS) hybrid

The graphene oxide–polystyrene microplastic (GO@PS) hybrid was prepared using a green methodology to mimic a natural process in a lab, as shown in Fig. 1. Graphene oxide nanosheets were purchased from Sigma Aldrich (USA) and after-usage flow cytometer (FACS) polystyrene beads (BD Life Sciences, USA) were used for the synthesis of the GO@PS hybrid. A floral extract of *Calotropis gigantea* (*C. gigantea*) was
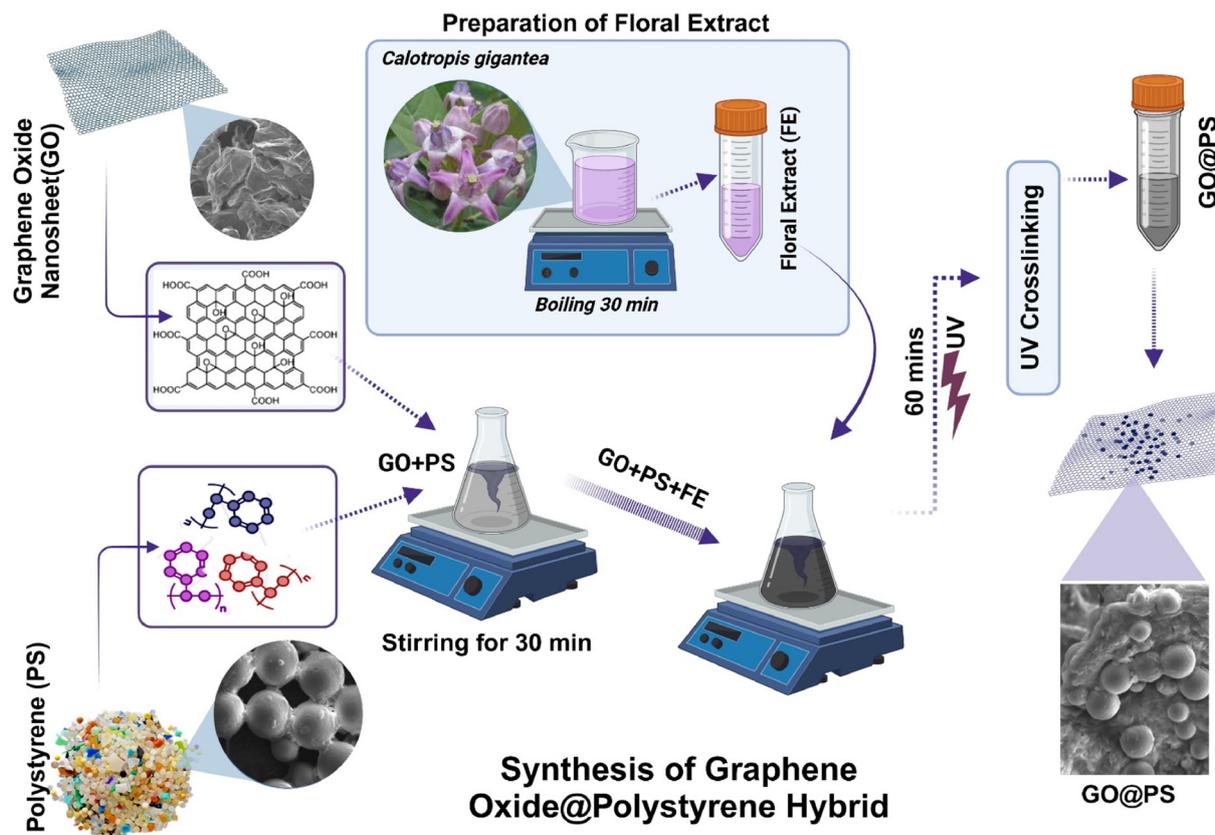
This journal is © The Royal Society of Chemistry 2025

Environ. Sci.: Nano, 2025, **12**, 1592–1608 | 1593

Fig. 1 Schematic displaying the green synthesis of the graphene oxide–polystyrene (GO@PS) hybrid.

used as a catalyzing agent. To obtain the floral extract, *C. gigantea* flowers were collected from premises near the School of Biotechnology, KIIT University, Bhubaneswar, India during the morning. The flowers were rinsed and the floral parts of the flowers were weighed (25 grams) followed by fine chopping them. They were then boiled in 500 mL of distilled water for 30 min till they showed a pink color. The solution was then cooled and filtered using a muslin cloth. Meanwhile, commercially purchased PS was suspended in DMSO to prepare a solution with a 1 mg mL^{-1} concentration, which was further diluted using MilliQ water to give a working solution of 100 μg mL^{-1}. Alongside this, a 10 mM solution of GO was prepared in MilliQ water. The synthesis reaction was set up by incubating the floral extract with GO (1 mM) and PS solution (100 μg mL^{-1}) in a ratio of 1:1 (V/V) with a final volume of 100 mL at 37 °C overnight. The reaction setup was kept under UV exposure in a UV cross-linker (30 min, twice) rotating condition at 100 rpm. Following incubation, the solution mixture was washed twice to remove any unused biomolecules in the solution.

2.2. Physiochemical characterization of the GO, PS, and GO@PS nano-hybrid

The GO, PS, and GO@PS nano-hybrid were characterized to determine their physicochemical properties using standard physical techniques. The visualization and size determination were performed by a scanning electron microscopy (SEM) system (Carl Zeiss, Germany) equipped with EDS (Ametek, Germany). The sample preparation for the SEM analysis was done by drying samples placed on silicon wafers, followed by applying a Pd/Au coating using a sputter counter. The hydrodynamic diameter and zeta potential were estimated using a Zetasizer (Malvern, UK) in Holtfreter (HF) medium. The GO@PS nano-hybrid was also characterized for assessing the molecular interactions in the hybrid through an *in silico* molecular docking approach. The docking was done using AutoDock Vina (Version 1.5.7)[34] with styrene (PS) as the ligand and GO as the receptor. The docking result was analyzed by identifying the ideal binding position with the lowest binding energy. The receptor and ligand were optimized using the AutoDock module of MGL Tools, and the grid dimension was set to 22 × 15 × 15 with a spacing of 1 Å. Post-docking analysis and visualization of the receptor–ligand interaction was performed with the help of Discovery Studio Visualizer[35] and ChimeraX.[36] For the 2D interactions plot, LigPlot+ was used. The 2D plots were derived from the receptor–ligand complexes with styrene as a ligand.

2.3. Zebrafish maintenance and embryo culture

The maintenance of the adult zebrafish was done with an overflow system purchased from Aquaneering, USA. The system was equilibrated with appropriate fish water during

maintenance (75 g NaHCO$_3$, 18 g sea salt, and 84 g CaSO$_4$ per 1000 mL).[37] The feeding of the fish was done twice a day with food constituting bloodworms. A 12 h light and dark cycle was maintained to ensure the photoperiodism. The breeding setup was arranged in a breeding box supplied by Aquaneering (USA) to obtain embryos. The setup was done by keeping male and female fish in a ratio of 2 : 1 overnight with a net partition, while removal of the partition was done in the morning to allow spawning the eggs. The viable embryos were collected and rinsed three times in HF medium. For further experimentation, the rearing of embryos was done in filter-sterilized HF medium. All the experiments were performed in compliance with the relevant laws and institutional guidelines of the Institutional Animal Ethics Committee (IAEC) at KIIT University. All the animal procedures were approved by the Institutional Animal Ethics Committee (IAEC) of KIIT University.

2.4. Toxicological assessment

In vivo toxicological assessment of the GO, PS, and GO@PS was done using the embryonic zebrafish model. For the experimental setup, 20 embryos were exposed to different concentration (25, 50, 100, 200, 500 µg mL^{-1}) of GO, PS, and GO@PS suspended in HF medium in a 24-well plate with a final volume of 500 µL for 72 h. The plate was kept at 28 °C ± 1 °C for a photoperiod comprising 12/12 h light/dark cycles. The morphological abnormalities were visualized using a stereomicroscope/fluorescence microscope (EVOS, Thermo Scientific). Morphological abnormalities, like notochord developmental defects, pericardial edema, tail deformities, and swollen yolks, were observed, and their frequency score was evaluated. The survivability rate was evaluated according to the test guideline of OECD 236 and was calculated as the frequency of live embryos after 72 h post-fertilization compared to in the untreated group. Determination of the hatching rate was estimated by the number of embryos hatched 72 h post-fertilization compared to the untreated group.[38] Heart rate was assessed by the heartbeat count per minute. All the experiments were done in triplicate and repeated three times in different days in fresh HF buffer.

2.5. Accumulation analysis

The comparative accumulation of GO, PS, and GO@PS on the embryos' surface was estimated using flow cytometry. The accumulation evaluation was done by measuring the mean side scatter by flow cytometry of the cellular suspension of embryos exposed to different concentrations of GO, PS, and GO@PS.[39] In brief, 72 h GO-, PS-, and GO@PS-exposed embryos were rinsed with sterilized HF buffer and sonicated to obtain single-cell suspensions. The single-cell suspensions were then analyzed using a flow cytometer (Attune focusing cytometer, Thermo Fisher Scientific, USA). Flow cytometric analysis was performed using the Attune acoustic focusing cytometer (Applied Biosystems, Life Technologies) equipped

with a 488 nm argon laser. Data analysis and presentation were performed with the help of FCS Xpress 6 (Denovo, CA, USA). The mean side scatter was measured and presented as a histogram for comparative analysis.

2.6. Assessment of cellular oxidative stress and apoptosis

The induction of cellular oxidative stress due to the exposure of GO, PS, and GO@PS was deduced through estimation of the reactive oxygen species (ROS) in cells through fluorescent microscopy and flow cytometry.[40] Cellular apoptosis was also analyzed using fluorescent microscopy and flow cytometry. All the treated and untreated zebrafish embryos[20] exposed to the samples at 72 h were rinsed with sterilized HF buffer and collected. For the fluorescent microscopy, all the untreated and treated embryos from different exposure setups were stained with 1.2 mg L^{-1} H$_2$DCFDA dye for 20 min for oxidative stress assessment, while staining with acridine orange was performed with a concentration of 5 µg ml^{-1} AO (dissolved in HF) for 20 min, followed by washing twice with HF buffer for the removal of extra staining agent. Images were captured using the green channel of an EVOS inverted fluorescence microscope (Thermo Fisher Scientific, USA) for comparing the induced oxidative stress and apoptosis in zebrafish embryos due to the exposure of different concentrations of GO, PS, and GO@PS nano-hybrid.

For flow cytometry analysis, the collected embryos were further sacrificed, and their cell suspension was prepared by mild sonication in HF buffer. Following sonication, the suspension was centrifuged at 5000 rpm for 10 min. Staining of the cell suspension was done using 1.2 mg L^{-1} H$_2$DCFDA dye for ROS analysis and acridine orange for apoptosis assessment for a duration of 20 min in the dark. Followed by staining, washing was performed with sterilized HF buffer to remove the extra staining agent. Flow cytometric analysis was performed using the Attune acoustic focusing cytometer (Applied Biosystems, Life Technologies) equipped with a 488 nm argon laser. Data analysis and presentation were performed with the help of FCS Xpress 6 (Denovo, CA, USA).[41] The fluorescent intensity of DCFDA in the ROS measurements was determined using the BL1 filter of the cytometer. For apoptosis assessment, the BL2 filter of the cytometer was used. All the readings were recorded in triplicate by taking embryos from three different plates and statistical analysis was performed using Graph Pad Prism 9.

2.7. *In silico* analysis

A computational approach was utilized to understand the interaction mechanism at the molecular level. For mechanistic toxicological analysis of the industrial GO nanosheet molecular interaction with Zhe1 (the hatching protein of zebrafish that is responsible for swelling and digesting the envelope (chorion), and also the growth and development of embryonic zebrafish) was checked *via* an *in silico* approach. To elucidate the mechanism of styrene nanotoxicity in zebrafish embryos, an *in silico* approach was

This journal is © The Royal Society of Chemistry 2025

Environ. Sci.: Nano, 2025, **12**, 1592–1608 | 1595

performed in view of the experimental results to investigate the probable interaction of polystyrene with Zhe1 proteins of the embryonic zebrafish responsible for the cellular changes. The interaction study was performed using AutoDock 4.2.6/AutoDock Tools 1.5.6 with industrial GO nanosheet and polystyrene (PS) as the ligands, and Zhe1 as the receptor protein. The structures of the industrial GO nanosheet and polystyrene were drawn with the help of ATB server. Furthermore, their geometry was optimized and also its energy was minimized using the ATB server. PMV was used for energy minimization in the receptor proteins. The parameters for industrial graphene oxide and polystyrene nanosheet were set in AutoDock 4.2.6. The grid dimensions were set to $38 \times 56 \times 46$ for GO–Zhe1 docking and $40 \times 58 \times 52$ for polystyrene docking, with a spacing of 1 Å for the protein receptors. The docking was performed for the ligand–receptor complex structure's molecular interaction and for identification of the optimal binding sites with the lowest binding energy and 0 rmsd value. Post-docking analysis was performed with the help of conformational clustering and visualized using Chimera and Discovery Studio Visualizer. 2D interaction plots were derived from the receptor complexes with industrial graphene oxide nanosheet as a ligand using LigPlot+.[42] GraphPad Prism v6.01 (San Diego, CA, USA) was used for the statistical analyses.

2.8. Statistical analysis

Statistical analysis was performed using GraphPad Prism v9 (San Diego, CA, USA). Respective confidential intervals were determined by non-linear fitting of the sigmoidal dose response curve. Data were analyzed by one-way ANOVA followed by Tukey/t-test with significance set at $P < 0.05$. Comparative results at each concentration were shown. Correlation analysis was performed between the ROS and apoptosis data by computing the non-parametric Spearman correlation.

3. Results and discussion

3.1. Green synthesis of the GO@PS hybrid

The formation of GO@PS was studied through a lab process mimicking a natural green synthesis. The GO@PS hybrid synthesis was carried out with the help of the floral extract of *Calotropis gigantea*, as shown in Fig. 1. A faint greenish color was observed after the incubation of GO and PS with the plant extract, which was further turned into a black suspension after exposure to UV light with the formation of a black precipitate indicating the formation of the GO@PS hybrid. The appearance of a greenish color can be reasoned to be due to the initial mingling of GO and PS with the reddish floral extract of the *C. gigantea*. Our previous studies have shown the presence of active biomolecules in the floral extract of *C. gigantea*, as determined through the gas chromatography mass spectrometry (GCMS) analysis,[43] like folic acid, 5-hydroxymethyl furfural bearing a –OH group,

Table 1 Compounds in floral extract of *Calotropis gigantea* determined by GC-MS analysis at different retention time (RT) peaks

Retention time	Compound identified
3.419	Pyranone
3.797	Dihydrobenzofuran
4.031	5-Hydroxymethylfufural
4.431	4-Mercaptophenol
4.483	4-Ethenyl-2-methoxyphenol
7.304	D-Mannose
9.656	Methyl hexadecanoate

saccharides, and 6-acetyl β-D-mannose (Table 1). The formation of a black precipitate as an indicator of the formation of the GO@PS hybrid could be attributed to the channeling of the reaction under UV exposure and with the aid of the biomolecules present in the floral extract of *C. gigantea*.[44,45]

3.2. Physicochemical characterization of GO@PS

Go, PS, and GO@PS were characterized for assessing their physicochemical properties using standard characterization techniques. The materials were visually characterized using a stereomicroscope. As shown in Fig. 2A, the GO@PS was clearly observed to be integrated with PS compared to the observed GO sheet and spherical PS alone. For further detailed visualization, SEM analysis was done. As shown in Fig. 2B, the GO was observed as a sheet structure while the PS had a spherical morphology. The GO@PS hybrid displayed the integration of PS with GO sheets. EDS analysis confirmed the presence of C, O, and Si indicating the presence of polystyrene and GO. However, a small amount of silicon was also found in the experimental setup (Fig. S1†), which could be attributed to the silicon wafer substrate. The size and stability of the materials were determined in aqueous media and HF buffer to estimate their hydrodynamic diameter and zeta potential. As shown in Fig. 2C, the hydrodynamic diameters of the GO, PS, and GO@PS were observed to be 1117.0 ± 374.0, 222.9 ± 22.6, and 1433.0 ± 268.0 nm. The increased diameter of GO@PS compared to GO could be reasoned to be due to the hybridization of PS with GO. The stability of the materials in the medium was checked through their zeta potential. As shown in Fig. 2D, the zeta potentials of GO, PS, and GO@PS were found to be -68.0 ± 16.8, -41.8 ± 7.0, and -47.3 ± 5.7 mV, indicating the stability of the materials and the hybrid material. The increased value in the case of GO@PS compared to GO could be attributed to the hybridization of PS with the GO. To understand the molecular and mechanistic details of the hybridization of GO and PS, a computational approach was taken through molecular docking analysis. Fig. 2E, S2, and Table S1† shows the molecular interaction of GO with the PS molecule, showing that the GO sheets interacted with PS molecules with the help of H-bonds having a bond length of 3 Å. The binding
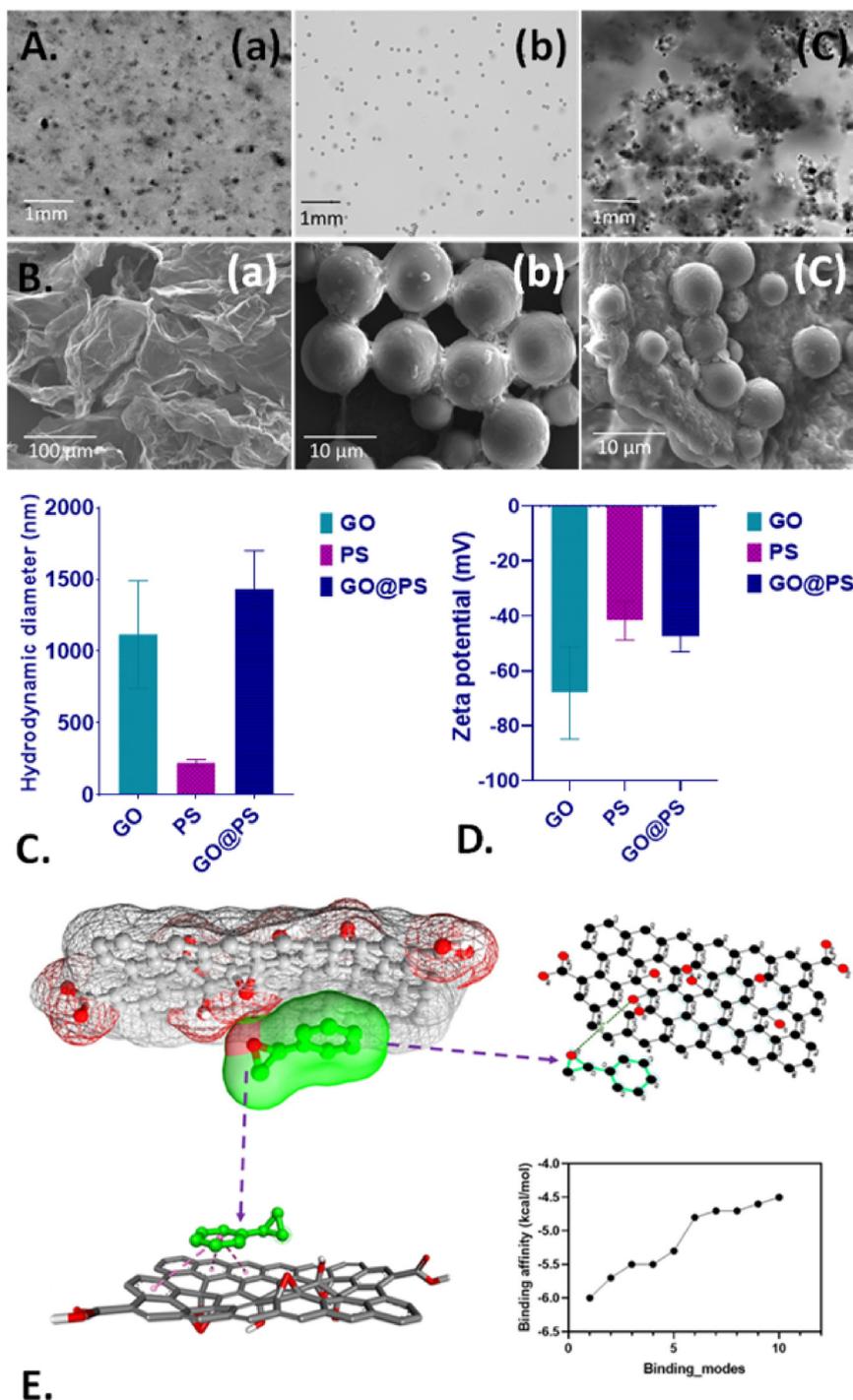
Fig. 2 Physicochemical characterization of the GO, PS, and GP@PS. (A) Optical microscopy images of (a) graphene oxide (GO), (b) polystyrene (PS), (c) GO@PS. (B) Scanning electron microscopy images of (a) GO, (b) PS, and (c) GO@PS. (C) Hydrodynamic diameters of GO, PS, and GO@PS determined by dynamic light scattering. (D) Zeta potentials of GO, PS, and GO@PS determined by dynamic light scattering. (E) Molecular interactions of GO and PS in GO@PS as determined by computational molecular docking.

affinities were predicted to be at different modes with an average binding energy of −6.0 kcal mol^{-1}. The computational data were in line with the experimental physicochemical characterization results of the GO@PS and advocated for the formation of the hybrid under the influence of abiotic parameters in the environment.

3.3. *In vivo* biotoxicity of GO, PS, and GO@PS with embryonic zebrafish

The *in vivo* biotoxicological impact of GO@PS was comparatively investigated by analyzing its exposure effect on physiological and cellular parameters in embryonic zebrafish.
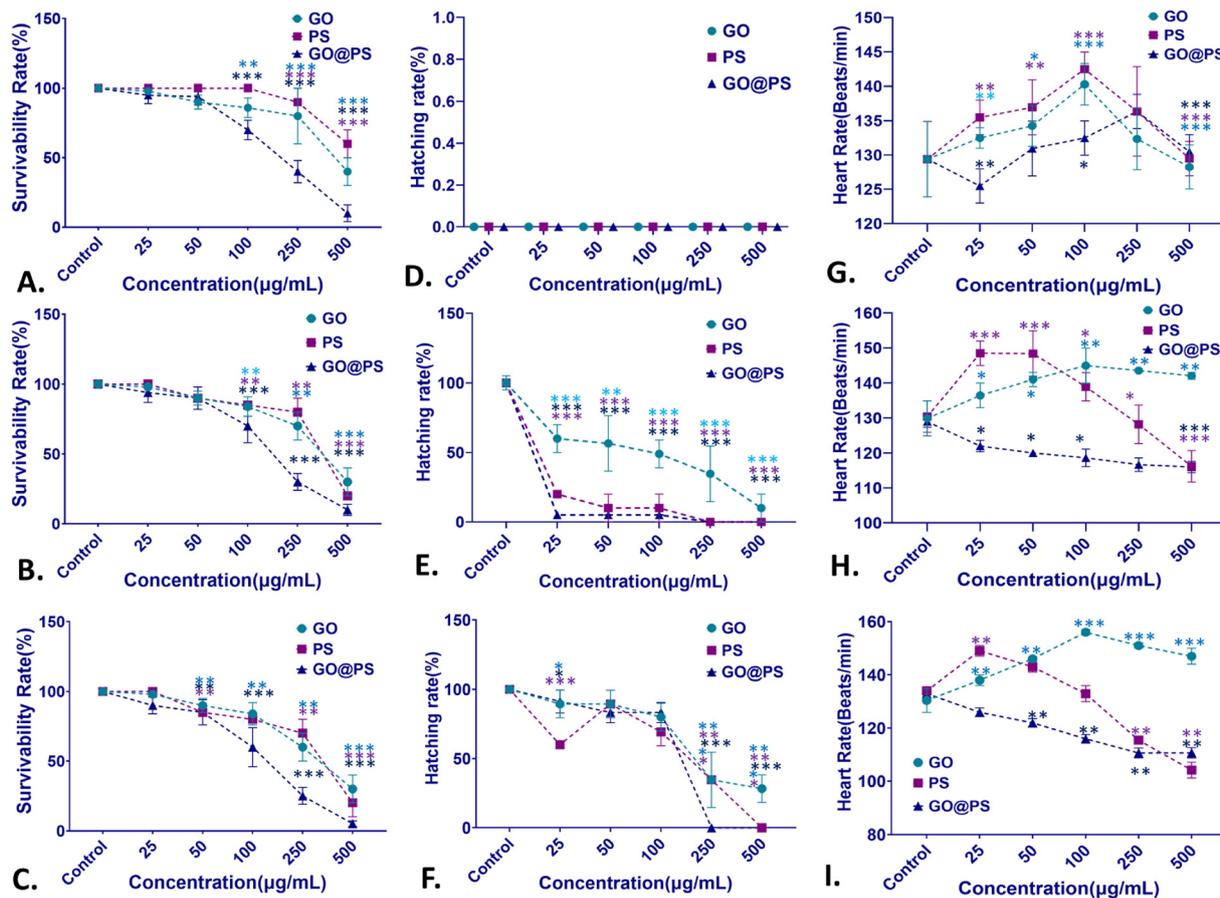
Fig. 3 *In vivo* physiological and toxicological effects of GO, PS, and GO@PS on embryonic zebrafish. (A)–(C) Survivability rate of zebrafish embryos exposed to different concentrations of GO, PS, and GO@PS. (D)–(F) Hatching rates of zebrafish embryos exposed to different concentrations of GO, PS, and GO@PS. (G)–(I) Heart rates of zebrafish embryos exposed to different concentrations of GO, PS, and GO@PS. The values are presented as the mean ± SD of 20 embryos in triplicate. All the experimental analysis was done in triplicate and three times independently. *$P > 0.5$, **$P > 0.01$, and ***$P > 0.001$ denote the compared significant change at each exposed concentration as obtained from *post hoc* analysis after one-way ANOVA.

As shown in Fig. 3A–C, exposure of the embryos to GO, PS, and GO@PS showed they had a concentration-dependent and time-dependent effect on survivability of the zebrafish embryos. At 24 h exposure, the embryos were 100% viable at a lower concentration exposure of GO (50 μg ml^{-1}, 100 μg ml^{-1}), which declined in the case of higher concentrations of 250 and 500 μg ml^{-1}. However, PS showed an impact of declining survivability of the embryos at higher concentration only. Interestingly, exposure of the embryos to the GO@PS hybrid caused a decrease in survivability at a lower concentration of 50 μg ml^{-1} to higher concentrations. After exposure for 48 and 72 h, a similar trend was observed, however the lethality of all the three materials were expressed at a higher rate. It was notable that at a very high concentration of 500 μg ml^{-1}, the survivability of the embryos was reduced to 20%. The LC50 values of the GO, PS, and GO@PS were calculated as 410.5, 768.4, and 210.6 μg ml^{-1} at 24 h. However, the values were reduced to 364.6, 353.2, and 187.4 μg ml^{-1} at 48 h of exposure. At 72 h, there was a sharp decline in values to 303.3, 341.2, and 121.4 μg ml^{-1} for GO, PS, and GO@PS. The results indicated a synergistic effect of

GO and PS in the declining survivability of the embryos. These results were in line the results observed in studies where the exposure of microplastics[46] and graphene oxide[47] showed their toxic effects in zebrafish in a concentration-dependent manner at the individual level. The comparative effect of GO, PS, and GO@PS could be attributed to combinatorial discrepancies in the physiological and metabolic effects in zebrafish embryos due to the exposure to GO, PS, and GO@PS.[48] To identify these effects, the hatching rate and heart rate were analyzed in embryos exposed to GO, PS, and GO@PS. As shown in Fig. 3D–F, a concentration-dependent decrease in hatching rate was observed in the embryos exposed to GO, PS, and GO@PS at 48 and 72 h of exposure. Comparatively, at 48 h of exposure, the embryos exposed to GO showed a gradual decrease in hatching rate, while it was significantly very low in the case of PS exposure. However, interestingly, the hatching rate was negligible and very low in the case of GO@PS exposure. A similar trend was followed at 72 h exposure in the case of GO, while the PS-exposed embryos were found to hatch at a slowly decreasing rate. However, in an interesting manner, the hatching rate of

the embryos exposed to GO@PS was significantly higher at lower concentration, which declined to 0% at higher concentrations of 250 and 500 μg ml^{-1}. The significant variation in the results could be attributed to the accumulation and attachment of the GO, PS, and GO@PS with the outer membrane of the chorion in the zebrafish embryos.[48] Further, to understand the comparative effect of the concentration-dependent exposure of GO, PS, and GO@PS on the physiology of the embryos, the heartbeat rate was observed in embryos exposed to the three types of
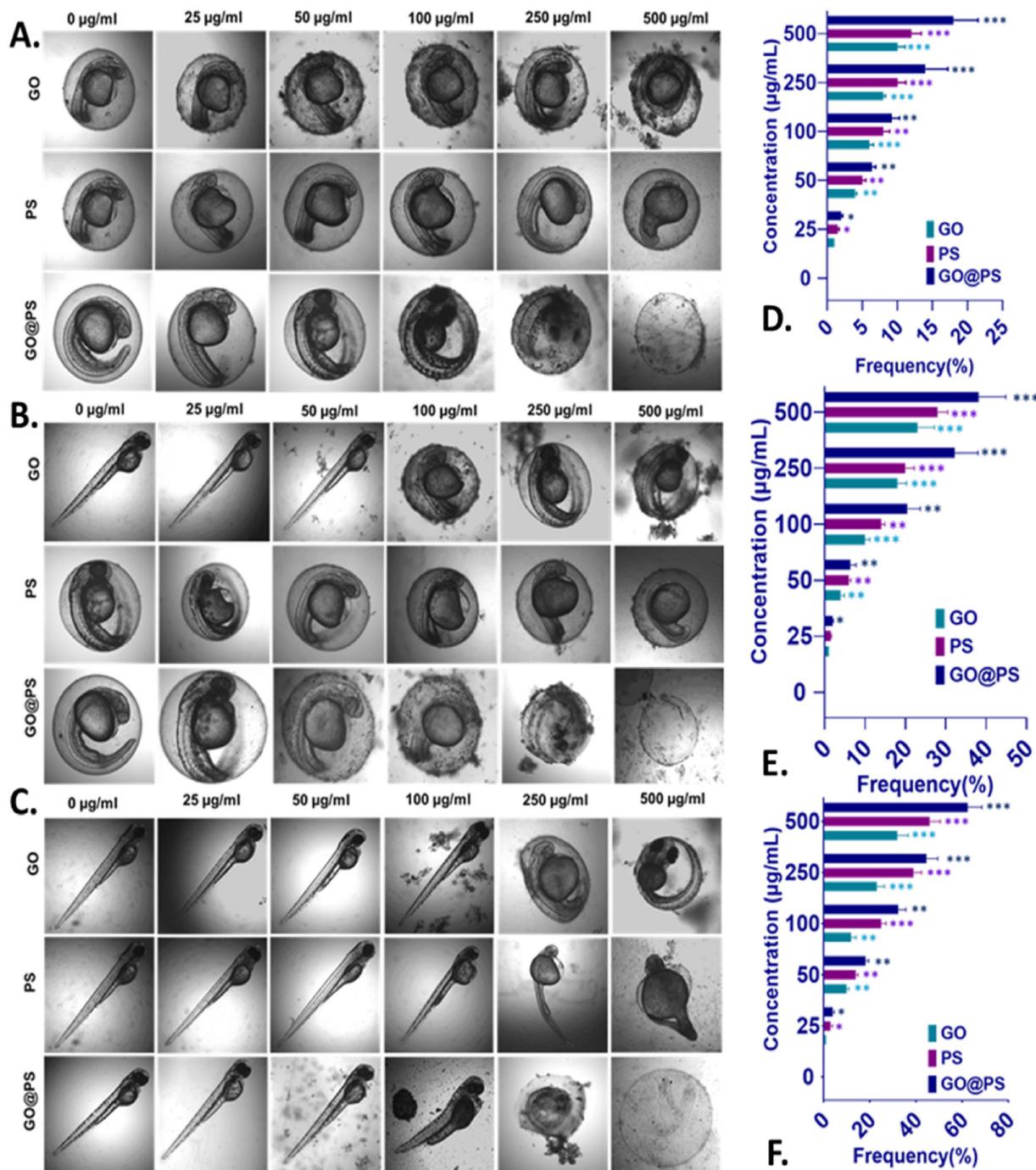
Fig. 4 *In vivo* toxicological effects of GO, PS, and GO@PS with embryonic zebrafish. Morphological abnormalities in zebrafish embryos exposed to different concentrations of GO, PS, and GO@PS exposed for (A) 24 h, (B) 48 h, and (C) 72 h. Abnormality frequencies in zebrafish embryos exposed to different concentration of GO, PS and GO@PS: (D) ABN: abnormal notochord, (E) PE: pericardial edema, (F) SY: swollen yolk. The values show the mean ± SD of 20 embryos in triplicate. All the experimental analysis was done in triplicate and three times independently. *$P > 0.5$, **$P > 0.01$, and ***$P > 0.001$ denote the compared significant change at each exposed concentration as obtained from *post hoc* analysis after one-way ANOVA.

This journal is © The Royal Society of Chemistry 2025

Environ. Sci.: Nano, 2025, **12**, 1592–1608 | 1599

materials. As shown in Fig. 3G–I, a gradual variation was observed in the heartbeat rates of the embryos exposed to GO at exposure times of 24, 48, and 72 h. However, in the case of PS exposure, the heartbeat rate was found to increase initially with the increase in concentration but decreased with high concentrations exposure. The trends of these results could be reasoned to be due to the initial high activity of the heart to adjust to the changed environment due to the accumulation

of PS around the embryos; however, with further increasing the concentration and exposure time the physiological system gets adjusted.[49] In the case of GO@PS exposure, the heartbeat rate of the embryos was observed to be increased after 24 h of exposure with the increase in concentration, and became normal again at higher concentration. However, after 48 and 72 h of exposure, the rate was found to be significantly declined. Interestingly, the heartbeat rate
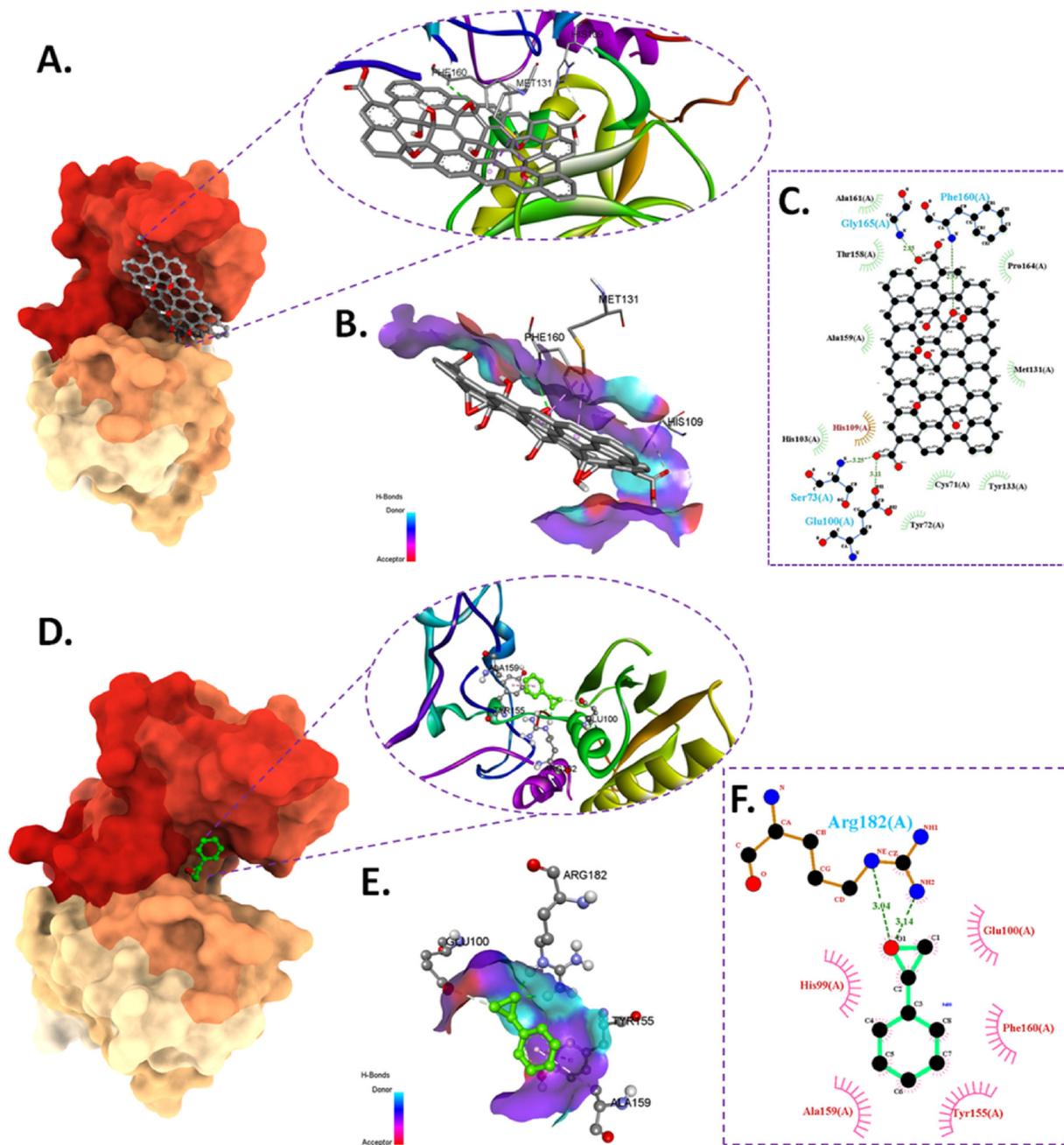

Fig. 5 Computational analysis of the molecular interactions of Zhe1a with GO and PS. (A) Conformational analysis of the interaction of Zhe1a enzyme with graphene oxide (GO) sheets. (B) Bond interaction analysis of GO with Zhe1a at the best conformational site. (C) LigPlot+ 2D presentation of the interaction bond with the amino acid residues of Zhe1a with GO. (D) Conformational analysis of the interaction of the Zhe1a enzyme with styrene (PS). (E) Bond interaction analysis of PS with Zhe1a at the best conformational site. (F) LigPlot+ 2D presentation of the interaction bond with the amino acid residues of Zhe1a with PS.

declination upon GO@PS exposure was lesser in comparison to the PS exposure at the same concentration. This result could be attributed to the synergistic effect of GO and PS accumulated at the surface of the chorion after their exposure.[48]

Further, the comparative impact of the physiological changes in embryos exposed to GO, PS, and GO@PS was speculated to show an overall effect in the form of morphological abnormalities. This hypothesis was checked by observing the morphology and scoring the physiological abnormalities, like abnormal notochord, pericardial edema, and swollen yolks, in the embryos exposed to GO, PS, and GO@PS. Fig. 4 shows the morphological abnormalities in the embryos exposed to GO, PS, and GO@PS for 24, 48, and 72 h. As shown in the figure, GO was observed to be accumulated at the chorion surface, while the attachment of PS and GO@PS was seen on the surface. A distinctive pericardial edema was observed at higher concentrations of GO, PS, and GO@PS. After 72 h exposure, the notochord abnormalities were clearly visible at higher concentrations of 100 and 250 μg ml^{-1} in all three cases. Moreover, swollen yolks were observed with higher acuteness with the increase in concentration and exposure time. Remarkably, the yolks were found to be absent in the case of exposure of GO@PS, indicating a very high acute effect of GO@PS at the molecular level. The frequencies of pericardial edema, abnormal notochord, and swollen yolks were found to be increased in a concentration-dependent manner; however, the degree and frequency of abnormalities were found to be higher and increasing in the case of GO@PS exposure compared to GO and PS.

These result were in line with the speculated hypothesis of the synergistic impact of the GO@PS hybrid on the embryos compared to GO and PS alone.[48] Moreover, the visual observation of the attachment of the GO, PS, and GO@PS confirmed the interaction of the materials with the chorion membrane. These result could be reasoned to be due to the abnormal hatching rate observed during analysis.[50] Previous literature has reported the role of metabolic proteins, like Zhe1a, in hardening the chorion membrane, leading to the phenomenon of hatching.[51] With reference to the literature, it could be found that the differential and comparative physiological and morphological abnormalities in embryos exposed to GO, PS, and GO@PS were due to the differential interactions of GO and PS individually as well as synergistically. To probe the further details, computational analysis was done to understand the molecular interaction of GO and PS with the metabolic protein GO@PS. As shown in Fig. 5A–C and Table 2, GO sheets were found to interact with Zhe1a through different amino acids, like Glu100 (3.11 Å) and Ser74 (3.25 Å), by polar interaction. Concurrently, it also interacts *via* Phe160 (2.93 Å) and Gly165 (2.85 Å) through hydrophobic bonds, as well *via* Met131 through pi–sigma bonds with a cumulative binding energy of −13.8 (kcal mol^{-1}). While styrene not only interacted with Zhe1 *via* Glu100 and Tyr155 through polar interactions, it also interacted with Zhe1 *via* Arg (3.14 Å) by electrostatic interaction and *via* Ala159 through hydrophobic bonds (Fig. 5D–F and Table 2). These results confirmed the impact of the interactions of GO and PS with the hatching protein and could be reasoned to have an influential effect on the structural and functional integrity of Zhe1a, leading to the abnormality in the hatching rate as well as other metabolic activities.[52] Moreover, this also supported the confirmation of the fact that in the case of the GO@PS hybrid, the combined interactive effect of GO and PS increased the severity of biotoxicity of the materials.

3.4. Cellular and molecular impacts of GO, PS, and GO@PS

The physiological and morphological analysis of the zebrafish embryos exposed to GO, PS, and GO@PS done experimentally and computationally confirmed the synergistic biotoxicity of GO and PS due to their accumulation at the surface of the chorion. Previous reports have suggested that the accumulation and internalization of nanomaterials at the surface of the chorion of zebrafish embryos can cause an abnormal induction of oxidative stress and apoptosis inside the embryos.[50] With reference to the previous reports, it was speculated that the accumulation and interaction of the GO, PS, and GO@PS materials at the surface leads to conformational changes in the chorion, which further creates disturbances inside the embryonic metabolic activities due to the hypoxic condition, leading to dysregulated oxidative stress and finally apoptosis of the cells.[53,54] This hypothesis was cross-validated through experimental quantitative and qualitative analysis using high-end techniques, like fluorescence microscopy and flow

Table 2 Details of ligand–protein interactions explaining the molecular interaction of Zhe1a with GO and PS

| Protein	Ligand	Binding energy (kcal mol^{-1})	Distance Å	Amino acid	Bond/interaction
Zhe1a	Graphene oxide nanosheet	−13.8	**3.11**	Glu 100	Polar interaction
			3.25	Ser 74	Polar interaction
			2.93	Phe 160	Hydrophobic bond
			2.85	Gly 165	Hydrophobic bond
			—	Met 131	Pi–sigma bond
	Polystyrene	−4.6	**3.68**	Glu 100	Polar interaction
			4.23	Tyr 155	Polar interaction
			3.14	Arg 182	Electrostatic interaction
			4.73	Ala 159	Hydrophobic bond
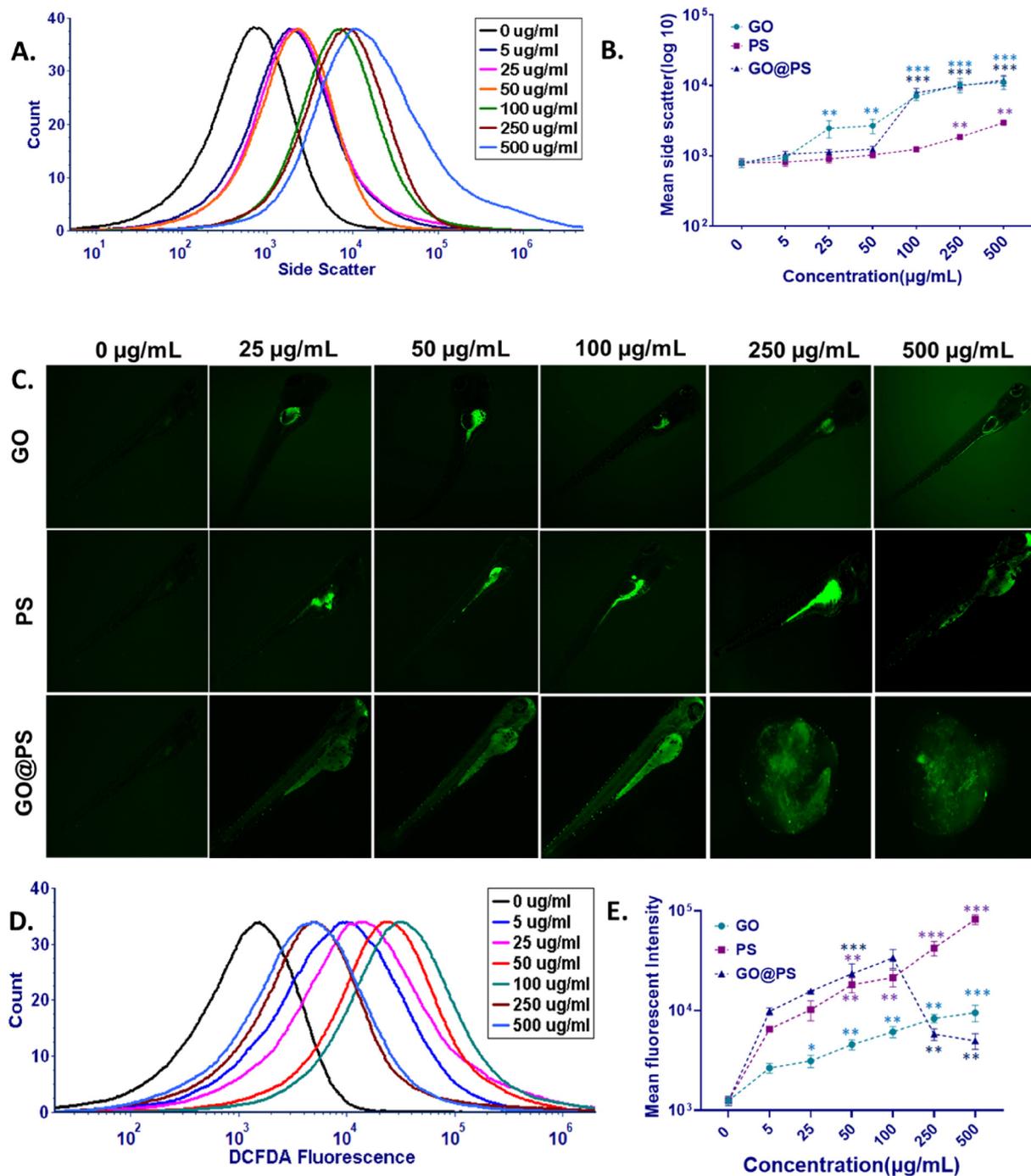
Fig. 6 Cellular impacts of GO, PS, and GO@PS. (A) Histogram presentation of the side scatter of cellular suspensions of 72 h-exposed zebrafish embryos exposed to different concentrations of GO@PS. (B) Comparative mean side scatter of cellular suspensions of 72 h-exposed zebrafish embryos treated with different concentrations of GO, PS, and GO@PS. (C) Fluorescence images of zebrafish embryos exposed to GO, PS, and GO@PS for 72 h stained with DCFDA for oxidative stress evaluation. (D) Histogram presentation of DCFDA green fluorescence in zebrafish cells exposed for 72 h with different concentrations of GO@PS. (E) Comparative analysis of the mean fluorescence intensity of DCFDA fluorescence in zebrafish cells exposed to GO, PS, and GO@PS for oxidative stress analysis. All the experimental analysis was done in triplicate and three times independently. $*P > 0.5$, $**P > 0.01$, and $***P > 0.001$ denote the compared significant change at each exposed concentration as obtained from *post hoc* analysis after one-way ANOVA.

cytometry. The comparative accumulation of GO, PS, and GO@PS was checked through side scatter analysis of the embryos exposed to the three materials.[53] As shown in Fig. 6A and S3,† the mean side scatter was found to be

increased with the increase in exposure concentration of GO, PS, and GO@PS. Comparatively, the mean side scatter was higher in the case of GO and GO@PS exposure than PS exposure (Fig. 6B). These results indicated the higher and

firmer accumulation of GO and GO@PS than PS. This outcome could be attributed to the higher surface areas of GO and GO@PS compared to the PS. The accumulation of GO, PS, and GO@PS was further be a definite cause for abnormalities arising from oxidative stress through the induction of the expression of reactive oxygen species (ROS).[38] The induction of ROS was analyzed through the measurement of the DCFDA fluorescent intensity in zebrafish embryos exposed to GO, PS, and GO@PS for 72 h. As shown in Fig. 6C, the fluorescent intensity of DCFDA was found to increase with the increase in concentration of GO, PS, and GO@PS, indicating the higher induction of ROS with the increase in exposure concentration to all three types of materials. However, remarkably, it was found that in the case of GO@PS exposure at higher concentrations of 250 and 500 $\mu g\ ml^{-1}$, the green fluorescence of DCFDA disappeared

quickly with the appearance of cellular debris inside the embryos. These results were further verified quantitatively using flow cytometry analysis of the DCFDA fluorescence intensity in embryos exposed to different concentrations of GO, PS, and GO@PS. As shown in Fig. 6D and S4,† the mean fluorescent intensity of DCFDA was found to increase with the increase in concentration of GO and PS exposure. While in the case of GO@PS exposure, the intensity was found to increase till 100 $\mu g\ ml^{-1}$ exposure and then decreased significantly at higher concentrations of 250 and 500 $\mu g\ ml^{-1}$ exposure (Fig. 6E). The analysis confirmed the observations from the fluorescent microscopy analysis. These results could be attributed to the formation of a hypoxic condition created inside the embryos due to the accumulation of GO, PS, and GO@PS at the chorion surface.[31,50] However, the exceptional and drastic decrease in ROS induction and the appearance of
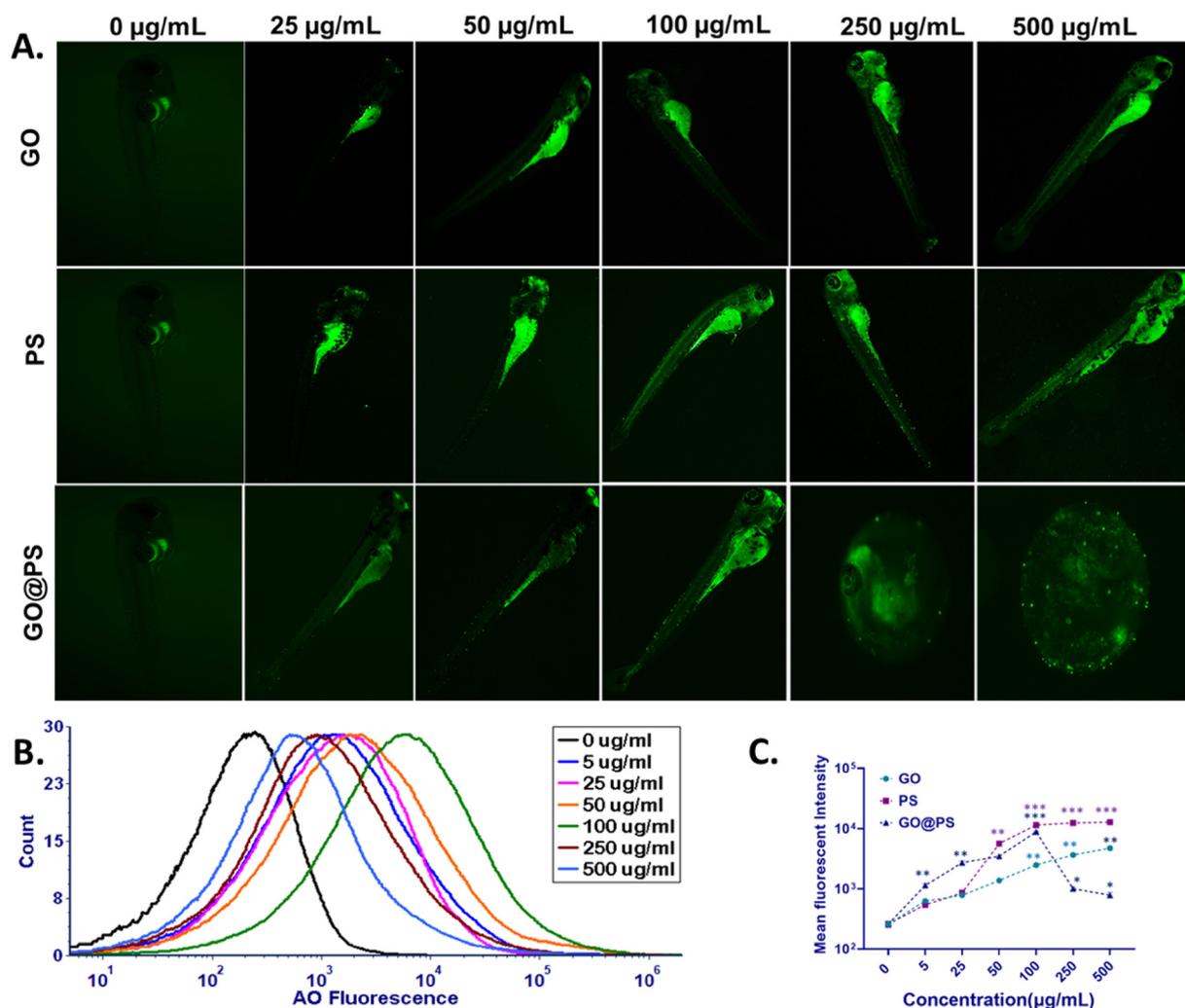

Fig. 7 Cellular impacts of GO, PS, and GO@PS. (A) Fluorescence images of zebrafish embryos exposed to GO, PS, and GO@PS for 72 h stained with acridine orange (AO) for apoptosis estimation. (B) Histogram presentation of acridine orange's green fluorescence intensity in zebrafish cells exposed for 72 h with different concentrations of GO@PS. (C) Comparative analysis of the mean fluorescence intensity of acridine orange fluorescence in zebrafish cells exposed to GO, PS, and GO@PS for apoptosis analysis. All the experimental analysis was done in triplicate and three times independently. *$P > 0.5$, **$P > 0.01$, and ***$P > 0.001$ denote the compared significant change at each exposed concentration as obtained from post hoc analysis after one-way ANOVA.

This journal is © The Royal Society of Chemistry 2025

Environ. Sci.: Nano, 2025, **12**, 1592–1608 | **1603**

cellular debris in the case of the higher-concentration exposure of GO@PS could be reasoned to be due to the severe hypoxic condition that occurred due to the synergistic blocking of the pores of the chorion, leading to a quick death of the cells.[31] The abnormalities in ROS induction generated inside the cells due to the external conditions have been reasoned to be one of the important factors in the induction of apoptosis in cells and cell death.[39,55] Accordingly, the dysregulation in ROS induction in zebrafish embryos exposed to GO, PS, and GO@PS was speculated to induce a discrepant apoptosis in embryos cells. This hypothesis was checked experimentally through the evaluation of acridine orange green fluorescence through fluorescent microscopy and flow cytometry in embryos exposed to GO, PS, and GO@PS. Fig. 7A shows the fluorescent images of zebrafish embryos exposed to GO, PS, and GO@PS stained with acridine orange for showing apoptosis induced due to ROS and other factors.[43] As could be seen from the image, the green fluorescent intensity of the acridine orange was found to be increased in embryos with the increase in exposure concentration of GO and PS. While, in case of GO@PS exposure the green fluorescence was found to be enhanced till 100 μg ml^{-1} exposure and then decreased drastically. These result depict the increasing apoptosis of the cells in embryos with the increase in exposure concentration of GO, PS, and GO@PS. However, the reduction in fluorescence of acridine orange at elevated concentrations of GO@PS (250 and 500 μg ml^{-1}) could be ascribed to the differential elevation and downregulation of reactive oxygen species (ROS) induction, as demonstrated by experimental investigations of oxidative stress.[39,56] The results were verified quantitatively through flow cytometry analysis. As shown in Fig. 7B and S5,† the mean fluorescent intensity was found to increase with the increase in exposure concentration of GO and PS, while there was clearly a left-shift in the histogram at a higher-concentration exposure of GO@PS, depicting the decrease in apoptotic cells in the embryos. These data were in line with the fluorescent microscopy results. The experimental and computational results indicated the synergistic biotoxicity of GO and PS expressed through the hybrid GO@PS. Moreover, it was depicted that the acuteness of the toxicity was higher in the case of the hybrid GO@PS. Previous literature on the *in vivo* toxicity of graphene oxide, its derivatives, and microplastics with different *in vivo* models has shown similar results for the concentration and size-based toxicity.[48] The defined study was thus in line with the previous reports and provides a novel emphasis of the facts describing the synergistic toxicity of graphene oxide and microplastics.

3.5. Mechanism

This study performed detailed mechanistic investigations on the toxicity of GO, PS, and GO@PS with the embryonic zebrafish model. The experimental investigations showed comparative and discrepant abnormalities at the morphological and physiological levels because of the accumulation and attachment of GO, PS, and GO@PS, while a detailed *in silico* analysis provided information on the intrinsic interaction of GO and PS for the formation of GO@PS and the molecular interactions of GO and PS with hatching proteins through different amino acids. With reference to the results and previous reports, the mechanism of the variable biotoxicity of GO, PS, and GO@PS can be defined as a consequence of the variability in accumulation and attachment of GO and PS at the surface of the chorion due to their chemical nature, which further showed variations in their intrinsic interactions with the chorion protein Zhe1a.[48] Moreover, the nature of possession of the acute biotoxicity of GO@PS compared to GO and PS can be defined by the combined and synergistic interaction of GO and PS with Zhe1a. These interactions lead to a blockage of the chorion pores and hardening of the chorion proteins, resulting in a variability of the hatching rate and the creation of hypoxic conditions inside the chorion.[50] In order to compensate the acute effect of the hypoxic conditions, a higher induction of ROS is promoted by exploiting the cellular respiratory machinery. However, metabolic disturbances occur at the molecular and cellular levels due to dysregulated oxidative stress, leading to cell death phenomena, like apoptosis. The significant variability in the structural integrity of GO, PS, and GO@PS leads to significant differences in the acuteness of the disturbances in metabolic processes. The detailed mechanism can be envisioned as occurring through the pathway illustrated in Fig. 8.

4. Conclusion

In brief, this study provides information about the synergistic biotoxicity of a graphene oxide and microplastic (polystyrene) hybrid (GO@PS) compared to graphene oxide (GO) and polystyrene (PS) microplastics alone. The hybrid was prepared by a green methodology under laboratory conditions to mimic the natural process. The hybrid material was hypothesized to possess toxicity at various levels, including developmental, morphological, cellular, and molecular, due to its variable physiochemical nature compared to GO and PS. The physicochemical characterization of the hybrid material was done experimentally to assess their size, hydrodynamic size, and zeta potential, and the estimations showed significant variability. The computational analysis elucidated the details about the intrinsic atomic interactions of GO and PS for the formation of GO@PS. The comparative mechanistic evaluation of the *in vivo* biotoxicity of GO, PS, and GO@PS was done using embryonic zebrafish as a test model. The results elucidated the higher toxicity of GO@PS to the zebrafish embryos in terms of their morphological, physiological, and developmental aspects through disturbances at the cellular and molecular levels. Moreover, the toxicity mechanism was deduced as a result of causing
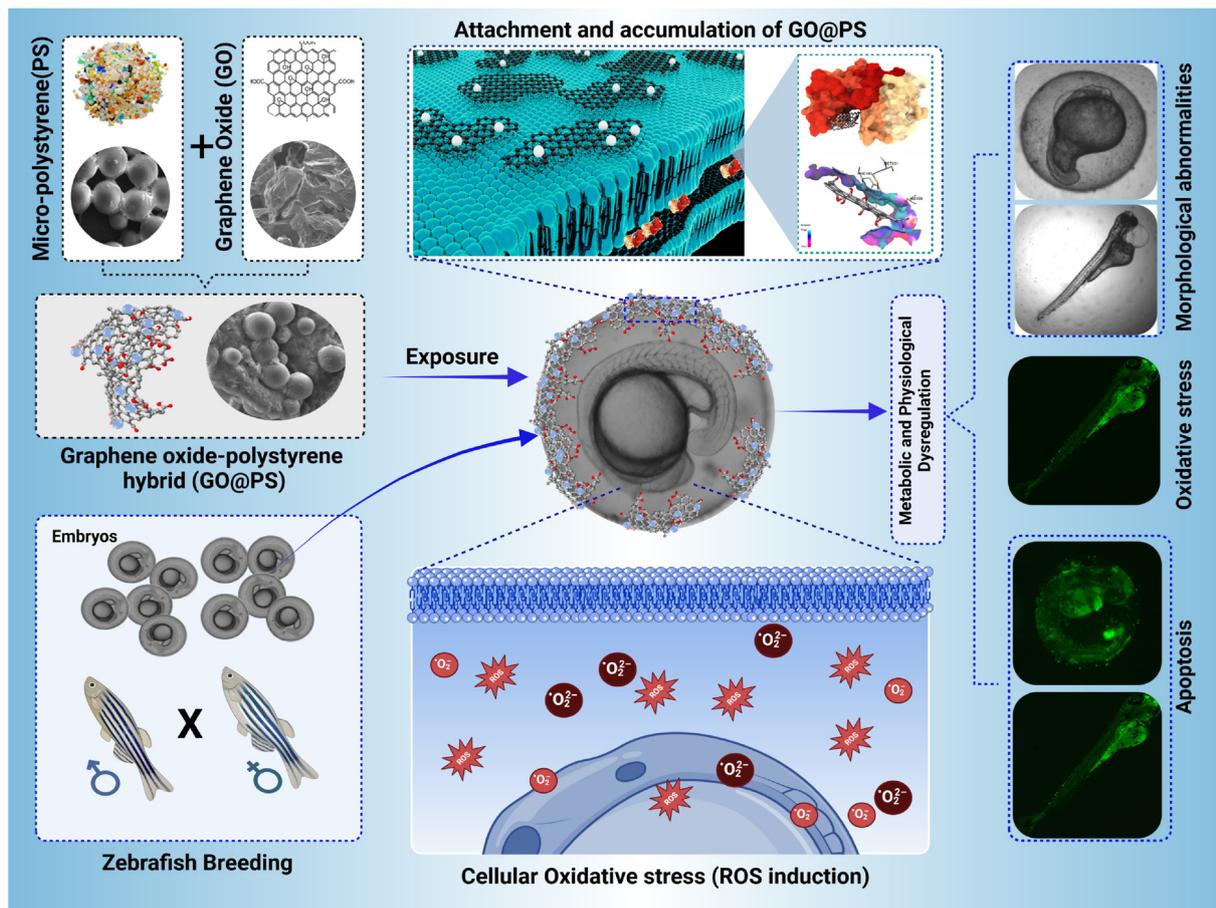
Fig. 8 Schematic of the mechanistic biotoxicity of the graphene oxide–polystyrene hybrid (GO@PS) toward zebrafish.

interferences in physiological phenomena, like oxidative stress, due to the creation of hypoxic condition led by the attachment and accumulation of GO@PS on the chorion of embryos, thus blocking the pores of the chorion. The results depicted the reason for the variability of the toxicity of the GO, PS, and GO@PS. The study provides valuable information about the comparative mechanism of *in vivo* biotoxicity induced by GO, PS, and GO@PS, suggesting the serious repercussions of their hazardous effect and the need for further research and steps to be taken in terms of the usage and disposal of graphene oxide and plastics for ensuring human health and the health of the environment.

Data availability

All the data supporting the study mentioned in this article have been presented through figures and tables. Additional data are available in the ESI† included in the submission.

Conflicts of interest

The authors declare that they have no known competing financial interests or personal relationships that could have appeared to influence the work reported in this paper.

Acknowledgements

References

1 N. Joudeh and D. Linke, Nanoparticle classification, physicochemical properties, characterization, and applications: a comprehensive review for biologists, *J. Nanobiotechnol.*, 2022, **20**, 262, DOI: **10.1186/s12951-022-01477-8.**

2 A. Sinha, F. Z. Simnani, D. Singh, A. Nandi, A. Choudhury, P. Patel, E. Jha, R. S. Chouhan, N. K. Kaushik, Y. K. Mishra, P. K. Panda, M. Suar and S. K. Verma, The translational paradigm of nanobiomaterials: Biological chemistry to modern applications, *Mater. Today Bio*, 2022, **17**, 100463, DOI: **10.1016/j.mtbio.2022.100463.**

3 J. Jeevanandam, A. Barhoum, Y. S. Chan, A. Dufresne and M. K. Danquah, Review on nanoparticles and nanostructured materials: History, sources, toxicity and regulations, *Beilstein J. Nanotechnol.*, 2018, **9**(1), 1050–1074.

This journal is © The Royal Society of Chemistry 2025

Environ. Sci.: Nano, 2025, **12**, 1592–1608 | **1605**

4   C. Chung, Y. K. Kim, D. Shin, S. R. Ryoo, B. H. Hong and D. H. Min, Biomedical applications of graphene and graphene oxide, *Acc. Chem. Res.*, 2013, **46**(10), 2211–2224.

5   T. Gao, Y. Qiang and Y. Liu, Applications of zero-dimensional carbon–based nanomaterials in bioimaging, in *Zero-Dimensional Carbon Nanomaterials*, Elsevier, 2024, pp. 515–576, available from: https://linkinghub.elsevier.com/retrieve/pii/B9780323995351000172.

6   H. Durmaz, A graphene-metal hybrid biosensor for SEIRA spectroscopy applications, *Opt. Commun.*, 2024, **550**, 130020, DOI: 10.1016/j.optcom.2023.130020.

7   Y. Hou, W. Wang and P. Bartolo, The effect of graphene and graphene oxide induced reactive oxygen species on polycaprolactone scaffolds for bone cancer applications, *Mater. Today Bio*, 2024, **24**, 100886, DOI: 10.1016/j.mtbio.2023.100886.

8   A. H. Luong, D. Istiqomah and W. C. Lin, Study of mechanical property and biocompatibility of graphene oxide/MEO2MA hydrogel scaffold for wound healing application, *Biomed. Eng. Lett.*, 2024, 537–548, DOI: 10.1007/s13534-024-00349-4.

9   A. T. Smith, A. M. LaChance, S. Zeng, B. Liu and L. Sun, Synthesis, properties, and applications of graphene oxide/reduced graphene oxide and their nanocomposites, *Nano Mater. Sci.*, 2019, **1**(1), 31–47.

10 D. Štular, N. Van de Velde, A. Drinčić, P. Kogovšek, A. Filipić, K. Fric, B. Simončič, B. Tomšič, R. S. Chouhan, S. Bohm, S. Kr. Verma, P. K. Panda and I. Jerman, Boosting Copper Biocidal Activity by Silver Decoration and Few-Layer Graphene in Coatings on Textile Fibers, *Glob. Chall*, 2023, 7, 2300113, DOI: 10.1002/gch2.202300113.

11 T. Arun, S. K. Verma, P. K. Panda, R. J. Joseyphus, E. Jha, A. Akbari-Fakhrabadi, P. Sengupta, D. K. Ray, V. S. Benitha, K. Jeyasubramanyan and P. V. Satyam, Facile synthesized novel hybrid graphene oxide/cobalt ferrite magnetic nanoparticles based surface coating material inhibit bacterial secretion pathway for antibacterial effect, *Mater. Sci. Eng., C*, 2019, **104**, 109932, DOI: 10.1016/j.msec.2019.109932.

12 H. Lin, T. Buerki-Thurnherr, J. Kaur, P. Wick, M. Pelin and A. Tubaro, *et al.*, Environmental and Health Impacts of Graphene and Other Two-Dimensional Materials: A Graphene Flagship Perspective, *ACS Nano*, 2024, **18**(8), 6038–6094, DOI: 10.1021/acsnano.3c09699.

13 A. T. Ta and N. Promchan, Microplastics in wastewater from developing countries: A comprehensive review and methodology suggestions, *TrAC, Trends Anal. Chem.*, 2024, **171**, 117537, DOI: 10.1016/j.trac.2024.117537.

14 K. Manikanda Bharath, A. L. Muthulakshmi and U. Natesan, Microplastic contamination around the landfills: Distribution, characterization and threats: A review, *Curr. Opin. Environ. Sci. Health*, 2023, **31**, 100422, DOI: 10.1016/j.coesh.2022.100422.

15 Z. Zhang, X. Wu, H. Liu, X. Huang, Q. Chen, X. Guo and J. Zhang, A systematic review of microplastics in the environment: Sampling, separation, characterization and coexistence mechanisms with pollutants, *Sci. Total Environ.*, 2023, **859**, 160151, DOI: 10.1016/j.scitotenv.2022.160151.

16 A. Choudhury, F. Z. Simnani, D. Singh, P. Patel, A. Sinha, A. Nandi, A. Ghosh, U. Saha, K. Kumari, S. K. Jaganathan, N. K. Kaushik, P. K. Panda, M. Suar and S. K. Verma, Atmospheric microplastic and nanoplastic: The toxicological paradigm on the cellular system, *Ecotoxicol. Environ. Saf.*, 2023, **259**, 115018, DOI: 10.1016/j.ecoenv.2023.115018.

17 A. Al Mamun, T. A. E. Prasetya, I. R. Dewi and M. Ahmad, Microplastics in human food chains: Food becoming a threat to health safety, *Sci. Total Environ.*, 2023, **858**, 159834, DOI: 10.1016/j.scitotenv.2022.159834.

18 M. Saeedi, How microplastics interact with food chain: a short overview of fate and impacts, *J. Food Sci. Technol.*, 2024, **61**(3), 403–413.

19 Y. Sun, C. Duan, N. Cao, X. Li, X. Li, Y. Chen, Y. Huang and J. Wang, Effects of microplastics on soil microbiome: The impacts of polymer type, shape, and concentration, *Sci. Total Environ.*, 2022, **806**, 150516, DOI: 10.1016/j.scitotenv.2021.150516.

20 H. C. Vo and M. H. Pham, Ecotoxicological effects of microplastics on aquatic organisms: a review, *Environ. Sci. Pollut. Res.*, 2021, **28**(33), 44716–44725.

21 C. Della Torre, E. Bergami, A. Salvati, C. Faleri, P. Cirino and K. A. Dawson, *et al.*, Accumulation and Embryotoxicity of Polystyrene Nanoparticles at Early Stage of Development of Sea Urchin Embryos Paracentrotus lividus, *Environ. Sci. Technol.*, 2014, **48**(20), 12302–12311, DOI: 10.1021/es502569w.

22 E. Besseling, B. Wang, M. Lürling and A. A. Koelmans, Nanoplastic Affects Growth of S. obliquus and Reproduction of D. magna, *Environ. Sci. Technol.*, 2014, **48**(20), 12336–12343, DOI: 10.1021/es503001d.

23 B. Jovanović, Ingestion of microplastics by fish and its potential consequences from a physical perspective, *Integr. Environ. Assess. Manage.*, 2017, **13**(3), 510–515, DOI: 10.1002/ieam.1913.

24 J. Martín, J. L. Santos, I. Aparicio and E. Alonso, Microplastics and associated emerging contaminants in the environment: Analysis, sorption mechanisms and effects of co-exposure, *Trends Environ. Anal. Chem.*, 2022, **35**, e00170, DOI: 10.1016/j.teac.2022.e00170.

25 S. H. Joo, Y. Liang, M. Kim, J. Byun and H. Choi, Microplastics with adsorbed contaminants: Mechanisms and Treatment, *Environ. Challenges*, 2021, **3**, 100042, DOI: 10.1016/j.envc.2021.100042.

26 S. K. Verma, M. Suar and Y. K. Mishra, Editorial: Green Perspective of Nano-Biotechnology: Nanotoxicity Horizon to Biomedical Applications, *Front. Bioeng. Biotechnol.*, 2022, **10**, 919226, DOI: 10.3389/fbioe.2022.919226.

27 S. K. Verma, A. Nandi, A. Sinha, P. Patel, S. Mohanty and E. Jha, *et al.*, The posterity of Zebrafish in paradigm of in vivo molecular toxicological profiling, *Biomed. Pharmacother.*, 2024, **171**, 116160, available from: https://linkinghub.elsevier.com/retrieve/pii/S0753332224000416.

28 S. K. Verma, A. Nandi, A. Sinha, P. Patel, E. Jha, S. Mohanty, P. K. Panda, R. Ahuja, Y. K. Mishra and M. Suar, Zebrafish (Danio rerio) as an ecotoxicological model for Nanomaterial induced toxicity profiling, *Precis. Nanomed.*, 2021, **4**, 750–781, DOI: **10.33218/001c.21978**.

29 J. Bhagat, L. Zang, N. Nishimura and Y. Shimada, Zebrafish: An emerging model to study microplastic and nanoplastic toxicity, *Sci. Total Environ.*, 2020, **728**, 138707, DOI: **10.1016/j.scitotenv.2020.138707**.

30 Y. Lu, Y. Zhang, Y. Deng, W. Jiang, Y. Zhao and J. Geng, *et al.*, Uptake and Accumulation of Polystyrene Microplastics in Zebrafish (Danio rerio) and Toxic Effects in Liver, *Environ. Sci. Technol.*, 2016, **50**(7), 4054–4060.

31 Y. Chen, X. Hu, J. Sun and Q. Zhou, Specific nanotoxicity of graphene oxide during zebrafish embryogenesis, *Nanotoxicology*, 2016, **10**(1), 42–52.

32 G. Audira, J. S. Lee, P. Siregar, N. Malhotra, M. J. M. Rolden, J. C. Huang, K. H. C. Chen, H. S. Hsu, Y. Hsu, T. R. Ger and C. Der Hsiao, Comparison of the chronic toxicities of graphene and graphene oxide toward adult zebrafish by using biochemical and phenomic approaches, *Environ. Pollut.*, 2021, **278**, 116907, DOI: **10.1016/j.envpol.2021.116907**.

33 H. Wang, Y. Wang, Q. Wang, M. Lv, X. Zhao, Y. Ji, X. Han, X. Wang and L. Chen, The combined toxic effects of polyvinyl chloride microplastics and di(2-ethylhexyl) phthalate on the juvenile zebrafish (Danio rerio), *J. Hazard. Mater.*, 2022, **440**, 129711, DOI: **10.1016/j.jhazmat.2022.129711**.

34 O. Trott and A. Olson, AutoDock Vina: inproving the speed and accuracy of docking with a new scoring function, efficient optimization and multithreading, *J. Comput. Chem.*, 2010, **31**(2), 455–461.

35 B. R. Brooks, C. L. Brooks III, A. D. Mackerell, L. Nilsson, R. J. Petrella, B. Roux, Y. Won, G. Archontis, C. Bartels, S. Boresch, A. Caflisch, L. Caves, Q. Cui, A. R. Dinner, M. Feig, S. Fischer, J. Gao, M. Hodoscek, W. Im, K. Kuczera, T. Lazaridis, J. Ma, V. Ovchinnikov, E. Paci, R. W. Pastor, C. B. Post, J. Z. Pu, M. Schaefer, B. Tidor, R. M. Venable, H. L. Woodcock, X. Wu, W. Yang, D. M. York and M. Karplus, CHARMM: The Biomolecular simulation Program, *J. Comput. Chem.*, 2009, **30**, 1545–1615.

36 E. F. Pettersen, T. D. Goddard, C. C. Huang, G. S. Couch, D. M. Greenblatt and E. C. Meng, *et al.*, UCSF Chimera—A Visualization System for Exploratory Research and Analysis, *J. Comput. Chem.*, 2004, **25**, 1605–1612, available from: **http://www.cgl.ucsf.edu/chimera/**.

37 H. Makkar, S. K. Verma, P. K. Panda, E. Jha, B. Das and K. Mukherjee, *et al.*, In Vivo Molecular Toxicity Profile of Dental Bioceramics in Embryonic Zebrafish (Danio rerio), *Chem. Res. Toxicol.*, 2018, **31**(9), 914–923, DOI: **10.1021/acs.chemrestox.8b00129**.

38 P. K. Panda, P. Kumari, P. Patel, S. K. Samal, S. Mishra and M. M. Tambuwala, *et al.*, Molecular nanoinformatics approach assessing the biocompatibility of biogenic silver nanoparticles with channelized intrinsic steatosis and apoptosis, *Green Chem.*, 2022, **24**(3), 1190–1210.

39 A. Ghosh, S. Singh, U. Saha, S. Jena, F. Z. Simnani, D. Singh, A. Gupta, A. Nandi, A. Sinha, T. Nayak, P. K. Rout, P. K. Panda, D. Singh, V. Raina and S. K. Verma, Proximal discrepancies in intrinsic atomic interaction determines comparative in vivo biotoxicity of Chlorpyrifos and 3,5,6-trichloro-2-pyridinol in embryonic zebrafish, *Sci. Total Environ.*, 2024, **913**, 169780, DOI: **10.1016/j.scitotenv.2023.16978**.

40 E. Jha, P. Patel, P. Kumari, K. K. Verma, P. K. Panda, P. S. Mohanty, S. Patro, R. S. Varma, Y. K. Mishra, N. K. Kaushik, M. Suar and S. K. Verma, In vivo molecular biocompatibility of Calotropis gigentea contrived smart Poly(N-isopropylacrylamide)-co-sulphonic-Silver microgel hybrid with embryonic Danio rerio inferred via intrinsic atomic physiological impacts, *J. Environ. Chem. Eng.*, 2023, **11**, 111183, DOI: **10.1016/j.jece.2023.111183**.

41 K. Kumari, A. Nandi, A. Sinha, P. K. Panda, A. Ghosh, S. K. Gouda, M. Suar, S. K. Verma and V. Raina, Biosurfactant-functionalized Silver nanoparticles infer intrinsic proximal interaction via Lysine and glutamic acid for reduced in vivo molecular biotoxicity with embryonic zebrafish through oxidative stress and apoptosis, *J. Environ. Chem. Eng.*, 2023, **11**, 110147, DOI: **10.1016/j.jece.2023.110147**.

42 S. K. Verma, E. Jha, P. K. Panda, P. Kumari, N. Pramanik and S. Kumari, *et al.*, Molecular investigation to RNA and protein based interaction induced in vivo biocompatibility of phytofabricated AuNP with embryonic zebrafish, *Artif. Cells, Nanomed., Biotechnol.*, 2018, **46**(sup3), S671–S684.

43 P. Kumari, P. K. Panda, E. Jha, K. Kumari, K. Nisha, M. A. Mallick and S. K. Verma, Mechanistic insight to ROS and Apoptosis regulated cytotoxicity inferred by Green synthesized CuO nanoparticles from Calotropis gigantea to Embryonic Zebrafish, *Sci. Rep.*, 2017, **7**, 16284, DOI: **10.1038/s41598-017-16581-1**.

44 P. Kumari, P. K. Panda, E. Jha, K. Kumari, K. Nisha and M. A. Mallick, *et al.*, Mechanistic insight to ROS and Apoptosis regulated cytotoxicity inferred by Green synthesized CuO nanoparticles from Calotropis gigantea to Embryonic Zebrafish, *Sci. Rep.*, 2017, **7**(1), 16284, available from: **https://www.nature.com/articles/s41598-017-16581-1**.

45 S. K. Verma, K. Nisha, P. K. Panda, P. Patel, P. Kumari and M. A. Mallick, *et al.*, Green synthesized MgO nanoparticles infer biocompatibility by reducing in vivo molecular nanotoxicity in embryonic zebrafish through arginine interaction elicited apoptosis, *Sci. Total Environ.*, 2020, **713**, 136521, available from: **https://linkinghub.elsevier.com/retrieve/pii/S0048969720300310**.

46 G. De Marco, G. O. Conti, A. Giannetto, T. Cappello, M. Galati and C. Iaria, *et al.*, Embryotoxicity of polystyrene microplastics in zebrafish Danio rerio, *Environ. Res.*, 2022, **208**, 112552, available from: **https://linkinghub.elsevier.com/retrieve/pii/S0013935121018533**.

47 Z. Chen, C. Yu, I. A. Khan, Y. Tang, S. Liu and M. Yang, Toxic effects of different-sized graphene oxide particles on zebrafish embryonic development, *Ecotoxicol. Environ. Saf.*, 2020, **197**, 110608, DOI: **10.1016/j.ecoenv.2020.110608**.

This journal is © The Royal Society of Chemistry 2025

Environ. Sci.: Nano, 2025, **12**, 1592–1608 | **1607**

48 A. M. Z. de Medeiros, L. U. Khan, G. H. da Silva, C. A. Ospina, O. L. Alves, V. L. de Castro and D. S. T. Martinez, Graphene oxide-silver nanoparticle hybrid material: an integrated nanosafety study in zebrafish embryos, *Ecotoxicol. Environ. Saf.*, 2021, **209**, 111776, DOI: **10.1016/j.ecoenv.2020.111776**.

49 M. Bangeppagari, S. H. Park, R. R. Kundapur and S. J. Lee, Graphene oxide induces cardiovascular defects in developing zebrafish (Danio rerio) embryo model: In-vivo toxicity assessment, *Sci. Total Environ.*, 2019, **673**, 810–820.

50 Z. Duan, X. Duan, S. Zhao, X. Wang, J. Wang, Y. Liu, Y. Peng, Z. Gong and L. Wang, Barrier function of zebrafish embryonic chorions against microplastics and nanoplastics and its impact on embryo development, *J. Hazard. Mater.*, 2020, **395**, 122621, DOI: **10.1016/j.jhazmat.2020.122621**.

51 N. Sizochenko, D. Leszczynska and J. Leszczynski, Modeling of interactions between the zebrafish hatching enzyme ZHE1 and a series of metal oxide nanoparticles: Nano-QSAR and causal analysis of inactivation mechanisms, *Nanomaterials*, 2017, **7**(10), 330, DOI: **10.3390/nano7100330**.

52 H. A. Elfawy, S. Anupriya, S. Mohanty, P. Patel, S. Ghosal and P. K. Panda, *et al.*, Molecular toxicity of Benzo(a)pyrene mediated by elicited oxidative stress infer skeletal deformities and apoptosis in embryonic zebrafish, *Sci. Total Environ.*, 2021, **789**, 147989, available from: **https://linkinghub.elsevier.com/retrieve/pii/S0048969721030606**.

53 S. K. Verma, A. Thirumurugan, P. K. Panda, P. Patel, A. Nandi, E. Jha, K. Prabakaran, R. Udayabhaskar, R. V. Mangalaraja, Y. K. Mishra, A. Akbari-Fakhrabadi, M. J. Morel, M. Suar and R. Ahuja, *et al.*, Altered electrochemical properties of iron oxide nanoparticles by carbon enhance molecular biocompatibility through discrepant atomic interaction, *Mater. Today Bio*, 2021, **12**, 100131, DOI: **10.1016/j.mtbio.2021.100131**.

54 P. Patel, P. K. Panda, P. Kumari, P. K. Singh, A. Nandi, M. A. Mallick, B. Das, M. Suar and S. K. Verma, Selective in vivo molecular and cellular biocompatibility of black peppercorns by piperine-protein intrinsic atomic interaction with elicited oxidative stress and apoptosis in zebrafish eleuthero embryos, *Ecotoxicol. Environ. Saf.*, 2020, **192**, 110321, DOI: **10.1016/j.ecoenv.2020.110321**.

55 H. U. Simon, A. Haj-Yehia and F. Levi-Schaffer, Role of reactive oxygen species (ROS) in apoptosis induction, *Apoptosis*, 2000, **5**(5), 415–418.

56 A. Choudhury, S. S. Lenka, A. Gupta, D. Mandal, A. Sinha, U. Saha, S. S. Naser, D. Singh, F. Z. Simnani, A. Ghosh, S. Kumari, A. Kirti, T. Parija, R. S. Chauhan, N. K. Kaushik, M. Suar and S. K. Verma, Controlled in vivo intrinsic detrimental effect of D-Limonene channelized by influential proximal interaction through apoptosis and steatosis in embryonic zebrafish (Danio rerio), *Sci. Total Environ.*, 2024, **949**, 175243, DOI: **10.1016/j.scitotenv.2024.175243**.

1608 | *Environ. Sci.: Nano*, 2025, **12**, 1592–1608

This journal is © The Royal Society of Chemistry 2025